Fuel 268 (2020) 117319

Contents lists available at ScienceDirect

Fuel

journal homepage: www.elsevier.com/locate/fuel

Full Length Article

Lithium leaching recovery and mechanisms from density fractions of an Illinois Basin bituminous coal

Wencai Zhang[a,*], Aaron Noble[a], Xinbo Yang[b], Rick Honaker[b]

[a] Department of Mining and Minerals Engineering, Virginia Polytechnic Institute and State University, Blacksburg, VA 24061, USA
[b] Department of Mining Engineering, University of Kentucky, Lexington, KY 40506, USA

ARTICLE INFO

Keywords:
Lithium
Coal
Calcination
Acid leaching
Kinetic analysis
Sequential chemical extraction

ABSTRACT

Lithium recovery from the density fractions of Baker (namely West Kentucky No. 13) seam coal was investigated in this study. Proximate and elemental analyses showed that lithium contents in the 1.8–2.2 SG and 2.2 SG sink fractions were 185 ppm and 150 ppm, respectively, which are significantly higher than the average content of coal sources (12 ppm) and coal ashes (66 ppm) worldwide. Moreover, due to the high lithium contents and mass distribution, nearly 90% of the lithium present in the Baker coal sample was distributed in the two density fractions. Direct leaching using a HCl solution resulted in less than 10% lithium recovery, which was due to nearly 90% of the lithium being associated with insoluble solids as determined by the results from sequential extraction tests. Calcination of both density fractions under 600 °C for two hours followed by leaching resulted in recovery increases in the range of 70% to 80%. The pyro-metallurgical pretreatment step converted most of the associated lithium minerals to more easy-to-leach forms such as carbonate and metal oxide. Based on mineralogy characterization and leaching test results, it was concluded that the positive effects of calcination on lithium leachability resulted from the dehydration and disintegration of kaolinite as well as dehydroxylation and expansion of muscovite/illite. An analysis of the leaching kinetics revealed that the leaching rate of lithium was controlled by interface transfer and diffusion across the product layer and was negatively impacted when the calcination temperature exceeded 600 °C due to sintering of the kaolinite.

1. Introduction

Lithium is a major high-tech metal and a crucial component in rechargeable batteries, fuel cells, and other electronic devices. Over the past 20 years, the growing ubiquity of personal electronic devices has caused tremendous growth in the demand of lithium metal with year-to-year production growth outpacing that of many other mineral resources (see Fig. 1). For example, data from the U.S. Geological Survey shows that the world total production of lithium increased from 69,000 tons in 2017 to 85,000 tons in 2018 – an increase of 23% in a single year [1]. This unabated growth in demand has caused many technology companies to evaluate the supply chain risks, and in turn, many international agencies and national governments have recently listed lithium as a critical and strategic commodity [2–4]. The conventional lithium supply chain includes primary production from either lithium-containing ores, such as spodumene and lepidolite, or aqueous resources, such as salt lake brines, geothermal brines, and seawater [5]. The US currently has only a single lithium producer, and majority of known lithium reserves reside in Chile with Australia, Argentina and China also controlling significant holdings [6]. Given the criticality of this resource and the importance to consumer and energy products, several researchers have recently assessed a number of alternative and unconventional sources of lithium [7,8].

Coal and coal byproducts are known to contain numerous trace elements, sometimes at elevated concentrations [9–11]. Since 2014, the U.S. Department of Energy has investigated the technical and economic feasibility of extracting rare earth elements (REEs, i.e. Sc, Y, and the lanthanides) from coal-related materials such as coal, coal refuse, coal combustion ash, and acid mine drainage [12–15]. Support from this program has led to the development of several novel processes, which were first evaluated at the bench scale and later validated at the pilot scale [13,15–23]. For example, Honaker et al. [16] has designed, constructed, and tested a unique REE recovery process that incorporates physical preparation, roasting, acid leaching, and selective precipitation. This process has been integrated into a pilot plant (https://www.youtube.com/watch?v=jR70j-MzWNE&t=3s) that has proven capability of continuously producing rare earth oxides concentrates exceeding 95% purity. Recent efforts in this program have expanded the

* Corresponding author.
E-mail address: wencaizhang@vt.edu (W. Zhang).

https://doi.org/10.1016/j.fuel.2020.117319
Received 22 November 2019; Received in revised form 2 February 2020; Accepted 3 February 2020

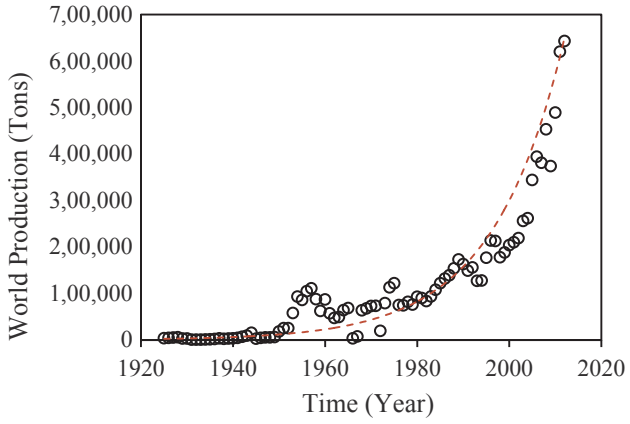

Fig. 1. World production of lithium as a function of time.

scope to critical materials such as lithium [24].

The average content of lithium in world coals and coal ashes were estimated to be around 12 ppm and 66 ppm, respectively. These average values are much higher than those of germanium, gallium, and selenium [25]; however, much lower than many conventional lithium ores. Despite the low average value, coal deposits that are high in lithium content have been reported in literature. For example, the Krylovsk and Verkhne-Bikinsk coal basins in the Russian Far East contain up to 0.22–0.65% Li_2O [9]. In the Jungar coalfield (Inner Mongolia, China), high contents of lithium were detected not only in the host-rocks but also in some coal benches [26,27]. The lithium present in the these coal deposits are primarily associated with clay minerals such as tosudite $[Na_{0.5}(Li,Al,Mg)_6((Si,Al)_8O_{18})(OH)_{12}{\cdot}5H_2O]$ and chlorite with composition intermediate between cookeite $[LiAl_4(AlSi_3O_{10})(OH)_8]$ and chamosite [9]. Finkelman et al. [28] conducted a systematic study to quantify the modes of occurrence of trace elements including lithium that are present in twenty US coals. The study found that more than 90% of the lithium was associated with clays and micas.

Recent studies by Zhang and Honaker [17,29] showed that REEs can be readily leached from coal refuse after carefully controlled calcination. The leaching performance for non-calcined samples and improperly calcined samples (i.e. calcined at a very high temperature) was significantly reduced. For example, under standard leaching conditions (1.2 M HCl, 1% solid concentration by weight, 75 °C reaction temperature, no calcination), only 10% of the REEs were leached from a Pocahontas No. 3 coarse refuse sample, even after 5 h of leaching time. Alternatively, when the sample was calcined at 600 °C for two hours prior to leaching, the recovery was increased to nearly 90% while the leaching duration was shortened to less than 15 min. In these studies, the positive impacts of calcination on the REE leachability were explained by two fundamental mechanisms: (1) hard-to-leach REE-bearing minerals were converted into more soluble forms; and (2) clay minerals especially kaolinite were dehydrated and decomposed causing the liberation of the encapsulated rare earth minerals [17,29,30].

As described above, geologic and speciation studies have shown that the lithium present in coals is closely associated with clay minerals. Moreover, recent experimental studies have shown that the calcination of coal refuse helps liberate trace elements, such as REEs, from the clay matrix. Together, these two observations suggest that proper calcination may also improve the leachability of lithium from coal-based materials. If implemented synergistically with an REE recovery process, the co-extraction of lithium may bolster the economic viability of the entire process and support a more sustainable use for coal waste. Unfortunately, investigations concerning lithium recovery from coals and coal-related materials have been rarely reported. To address this knowledge gap, this communication describes an experimental study where calcination and acid leaching tests were performed on different density fractions of the Baker seam coal of the Illinois Basin to evaluate the viability of lithium extraction. Leaching kinetic analysis and sequential chemical extraction were conducted to explain the calcination and acid leaching mechanisms. Systematic understandings of lithium extraction from the materials were ultimately achieved.

2. Material and methods

2.1. Material

Two barrels of the feed material reporting to a coal preparation plant processing Bake seam coal were representatively collected from a conveyor belt using a belt-sweep sampler. The sample was air-dried and the material coarser than 10 mm was obtained by dry sieving. The oversize fraction was density fractionated using density medium baths of 1.4 specific gravity (SG), 1.8 SG, and 2.2 SG, which were prepared by dispersing the required amounts of ultrafine magnetite in water to achieve the desired medium SG. After separation, the resultant four SG fractions were air-dried at room temperature and pulverized to a top size of 0.18 mm using a jaw crusher and a hammer mill. The pulverized materials were used as feedstocks for the calcination and lithium recovery tests.

The chemicals used in this study were at least ACS grade and purchased from Thermal Fisher Scientific, USA. Trace metal grade acids were used for the acid leaching and sequential chemical extraction tests as well as the solid sample digestions. The water used in the experiments was of type I purity with a resistivity of 18.2 MΩ·cm.

2.2. Methods

2.2.1. Calcination test

The samples were calcined at 400 °C, 600 °C, 750 °C, and 900 °C for two hours in a muffle furnace following procedures similar to those described by Zhang and Honaker [17]. For each batch of calcination, six crucibles containing 30 g of solid (5 g per crucible) were placed in the furnace. The temperature in the furnace was elevated from room temperature to the calcination temperatures at a rate of 10 °C/min. After calcination, the furnace was automatically cooled to room temperature, which took around 12 h. A static air condition was used during the overall calcination process.

2.2.2. Acid leaching test

Acid leaching tests were performed on both the raw and the calcined samples under uniform conditions, namely, 10 g/L solids concentration, 1.2 M hydrochloric acid, 75 °C reaction temperature, and 300 min reaction duration. The detailed testing procedures can be found in a prior communication [29]. Representative samples were taken from the slurry at different time intervals from the start of the leaching process up to a total period of 5 h (i.e., 5 min, 15 min, 30 min, 45 min, 60 min, 90 min, 2 h, 3 h, 4 h, and 5 h).

The element-by-element leaching recovery was determined by back-calculating the elemental feed assay (E_f, ppm) using the following equation:

$$E_f = 100 \times (C_s \times m_s + C_l \times V_l) \times m_i/(m_i - m_m)$$

where C_s and C_l represent the elemental concentrations (ppm, representing mg/kg for solid and mg/L for liquid) in the solid residue and final leachate, respectively; m_s (kg) weight of the leaching solid residue; V_l (liter) volume of the final leachate; m_i (kg) weight of the total leaching slurry; and m_m (kg) weight of all the representative samples collected during the leaching process. The difference between the back-calculated contents and the values measured directly using an inductively coupled plasma optical emission spectrometry (ICP-OES) were within ± 5%, indicating minor experimental errors.

Next, the element-by-element leaching recovery (R_i, %) was calculated using the following equation:

$$R_i = 100\% \times C_i \times V/(E_f \times 0.01) \quad (2)$$

where C_i (ppm) represents elemental concentrations in the filtrates collected during the leaching process, V volume of the feed solution (1 L), and E_f (ppm) the back-calculated elemental contents in the feed solids. All REE content values in the solids are reported based on a dry whole sample basis. Three duplicates were performed on the raw materials and the standard variances in the metal recoveries were less than 3%.

2.2.3. Sequential chemical extraction test

In prior studies, sequential chemical extraction (SCE) has been used as an indirect method to determine the mode of occurrence of trace elements [28,31,32]. In the SCE process, the solid specimen is sequentially reacted with a series of lixiviants under increasingly aggressive conditions. This procedure enables the extraction of only a specific mode of trace elements in each step. By measuring trace element concentration in the liquid obtained after each extraction, the distribution of trace elements in the different solid phases can be quantified.

In this study, SCE was performed to quantify the modes of occurrence of lithium in both the raw and calcined materials. The SCE procedure was formulated based on the protocols used for coal fly ash [32–34]. As shown in Fig. 2, the lithium present in the samples was classified into five different modes of occurrence, namely, 1) ion-exchangeable, 2) carbonate, 3) metal oxide, 4) acid soluble, and 5) insoluble, by reacting with magnesium chloride ($MgCl_2$), sodium acetate (CH_3COONa), acetic acid (CH_3COOH), nitric acid (HNO_3), and aqueous regia plus hydrofluoric acid (acid digestion) solutions, respectively. The addition of hydroxylamine hydrochloride ($NH_2OH{\cdot}HCl$) in the third step ensures that oxides of reducible metals such as iron and manganese are completely dissolved [32]. Two density fractions of the Baker coal (i.e., 1.4 SG float and 2.2 SG sink material) were selected for the test since they represented low- and high-density fractions, respectively. The SCE procedure is not directly effective for low ash content coals since the organic matter cannot be dissolved. Therefore, for the 1.4 SG float material, SCE was only performed on its calcination products. Three duplicates were performed for a selected material and the standard variances in the fractions of the different modes of occurrence were 2.44%, 1.51%, 2.27%, 5.24%, and 0.14%, respectively.

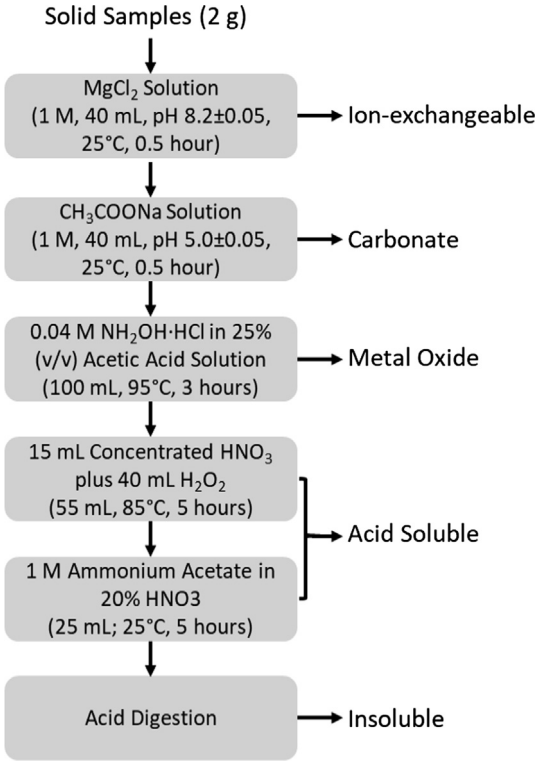

Fig. 2. Sequential chemical extraction procedure that was used for quantifying the modes of occurrence of lithium in the Baker SG fractions.

2.2.4. Sample characterization

Proximate analyses of the calcined and non-calcined samples were performed following the ASTM D5142 standard [35]. X-ray diffraction (XRD) was performed for mineralogy characterization using a Bruker-AXS D8 DISCOVER diffractometer that was configured in a parallel beam geometry with Cu-Kα radiation. XRD patterns were recorded over a 2θ range of 5°–70° with a step size of 0.02°. XRD patterns were analyzed using DIFFRAC, a commercial software developed by Bruker Corporation. Scanning electron microscope (SEM) analyses were performed on the calcination products to investigate the morphological changes caused by calcination.

Liquid samples generated during the tests were directly analyzed using ICP-OES equipment manufactured by Thermal Fisher Scientific, USA. Solid samples were first ashed following the ASTM D5142 standard [35] and then digested using aqua regia plus hydrofluoric acid. The elemental composition in the solid was then calculated based on the ICP-OES measurement of the solution generated by acid digestion. Further details on the acid digestion and ICP-OES analysis are provided by Zhang and Honaker [36]. For each batch of digestion, a standard solid sample supplied by the National Institute of Standards and Technology (NIST) of the U.S. Department of Commerce was digested together with the experimental solid samples. Analysis results were accepted if differences between the measured contents and the values provided by the supplier were ± 10%. The ICP-OES unit was calibrated using six standards prepared at the following concentrations: 0 ppm, 0.05 ppm, 0.5 ppm, 1 ppm, 5 ppm and 10 ppm. The calibration was verified by two independently sourced check standards, i.e., continuing calibration verification (CCV) and continuing calibration blank (CCB), every 10 samples. The lithium recovery for these check standards was ± 10% RSD. The detection limit of the method developed using the ICP-OES for lithium concentration measurement was 0.0033 ppm. A duplicate sample was chosen at random and run through the entire process to verify repeatability every 40 samples.

3. Results and discussion

3.1. Lithium content distribution

Proximate analysis showed that the 1.4 SG float, 1.4–1.8 SG, 1.8–2.2 SG, and 2.2 SG sink fractions of the Baker coal contained 6.38%, 23.53%, 73.29%, and 86.49% of ash, respectively (see Table 1 and Fig. 3 (a)). The majority of the material was distributed in the 2.2 SG sink fraction (59.9%), followed by the 1.4 SG float (17.5%) and the 1.4–1.8 SG (16.4%) fractions. Only 6.3% of the material reported to the 1.8–2.2 SG fraction. The lithium contents and distributions in the different SG fractions are shown in Fig. 3 (b). When reported on an ash basis, the maximum lithium content occurred in the 1.4–1.8 SG fraction (247 ppm); however, the content was reduced to 61 ppm when assessed

Table 1
Proximate analysis results of the different specific gravity fractions of the Baker coal.

Sample	Moisture (%)	Volatile (%)	Fixed carbon (%)	Ash content (%)	Total (%)
1.4 SG Float	2.19	36.92	54.52	6.38	100
1.4–1.8 SG	2.08	30.57	43.82	23.53	100
1.8–2.2 SG	1.98	14.12	10.61	73.29	100
2.2 SG Sink	1.78	10.79	0.94	86.49	100

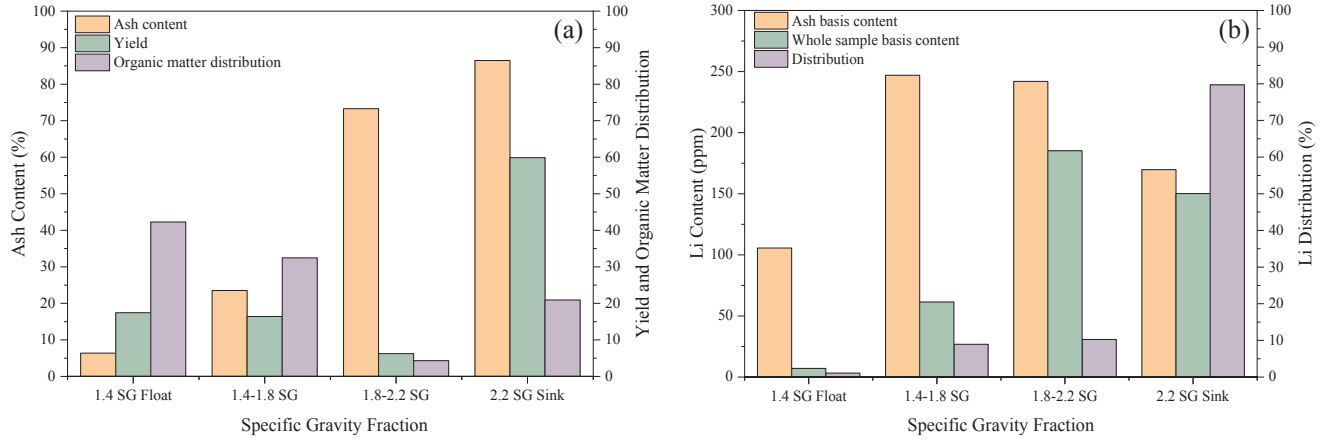

Fig. 3. Analyses of the different specific gravity fractions of the Baker material: (a) Ash content, yield, and organic matter distribution; (b) Lithium content and distribution.

on a whole sample basis. Moreover, the 1.8–2.2 SG and 2.2 SG sink fractions contained 185 ppm and 150 ppm of lithium, respectively, on a dry whole sample basis. These values are much higher than the low ash content fractions (e.g., 7 ppm of Li present in the 1.4 SG float). Due to the higher lithium contents and mass distributions in the high-density fractions, the majority of the lithium mass was found to be distributed in the fractions heavier than 1.8 SG. As shown in Fig. 3(b), the amount of lithium associating with the 2.2 SG sink and 1.8–2.2 SG fractions accounted for nearly 90% of the total lithium. Given this mass distribution, an optimal lithium recovery process should target the higher ash content coal refuse materials. This approach is preferred for many coal producers as it permits waste utilization without sacrificing the value of the clean coal.

3.2. Lithium leaching performance

For comparison purposes, acid leaching tests using 1.2 M HCl were performed on all SG fractions rather than just the high-density fractions that contain a majority of the lithium mass. Fig. 4(a)-(d) show lithium leaching recovery data as a function of leaching time for different SG fractions and calcination temperatures. Lithium recovery values for the as-received/raw materials were notably low (less than 10%), even at long leaching durations. The data appears to show a trend with lower SG fractions producing lower overall recovery values. In the case of the lightest SG fraction (1.4 SG float material), the leaching recovery of lithium was negligible, which may be due to the encapsulation of lithium in the organic matrix in forms of either complexation with organic matter or association with inorganic matter occurring in the organic matrix.

Given these low recovery values, blank calcination (i.e. calcination without additives) was used to pretreat the materials prior to acid leaching. As shown in Fig. 4(a)–(d), the lithium recoveries in all cases were significantly increased due to calcination. For example, less than 3% of the lithium was leached from the 1.4–1.8 SG fraction of the raw material; however, after calcination at 600 °C, the final recovery increased to nearly 80%. A comparison between the leaching results of the raw and the calcined materials showed that 60 to 80 absolute percentage point increases for all the four fractions by calcination. In addition, among the investigated temperatures, calcination at 600 °C provided maximum final lithium recoveries for all the SG fractions. Under a calcination temperature of 900 °C, the recovery values were reduced to less than 20%.

3.3. Modes of occurrence of lithium

Sequential chemical extraction tests were performed on the 600 °C, 750 °C, and 900 °C calcination products of the 1.4 SG float and 2.2 SG sink materials as well as the raw 2.2 SG sink material. As shown in Fig. 5 (a) and (b), a considerable portion of the lithium present in the 2.2 SG sink raw material occurred as an insoluble form, which explained the low recoveries obtained in the acid leaching tests (see Fig. 4). However, after calcination under 600 °C for two hours, the fraction of insoluble lithium was significantly reduced from 91% to 20%, indicating the conversion of the insoluble lithium into a more soluble form. This result corresponded to increases in the ion-exchangeable, carbonate, metal oxide, and acid soluble fractions (from 0.8% to 15%, 0.6% to 10%, 3% to 28%, and 5% to 27%, respectively). In the acid leaching tests, the solid was reacted with 1.2 M HCl under 75 °C for five hours, and thus all of the lithium occurring as ion-exchangeable, carbonate, and metal oxide forms should have been dissolved plus some of the acid soluble lithium, agreeing with the relatively high leach recovery value (nearly 70% after five hours of interaction). As shown in Fig. 5(b), the acid soluble and insoluble fractions increased when the calcination temperature exceeded 600 °C, and the insoluble fraction increased to nearly 80% in the 900 °C calcined sample. Therefore, excessive calcination treatment caused deleterious impacts on the extraction of lithium (see Fig. 4(d)). For the 1.4 SG float material, calcination showed similar effects on the modes of occurrence of lithium as the 2.2 SG Sink material in the temperature range of 600–900 °C. As shown in Fig. 5(a), the insoluble lithium only accounted for 23% of the total lithium present in the 600 °C calcination product of the 1.4 SG float material, whereas the insoluble fraction raised to 71% when the material was calcined under 900 °C for two hours. This finding also agreed with the acid leaching test results (see Fig. 4(a)).

The sequential chemical extraction results showed that nearly 90% of the lithium in the 2.2 SG sink material occurred in an insoluble form. To expound on these experimental results, Fig. 6(a) and (b) show the mineralogical analysis as determined by XRD. The major mineral phases in the raw materials included quartz, clays (kaolinite, illite, and muscovite), and pyrite. Trace amounts of anatase and calcite were also detected in the 1.4 SG float material. In the sequential extraction process, the easy-to-dissolve minerals such as pyrite and calcite were likely dissolved after the fourth step where strong acidic and oxidizing conditions were used. Therefore, the insoluble residue generated from the fourth step likely included quartz and clays. In addition, Fig. 6 (a) and (b) shows that quartz was unaffected by calcination, which is sufficient evidence to exclude the possibility that lithium was associating with quartz in the Baker materials. Based on the above discussion, it can be concluded that clay minerals are the major host phases for lithium in the Baker material especially the high-density fractions. This conclusion agrees with the study reported by Finkelman et al. [28].

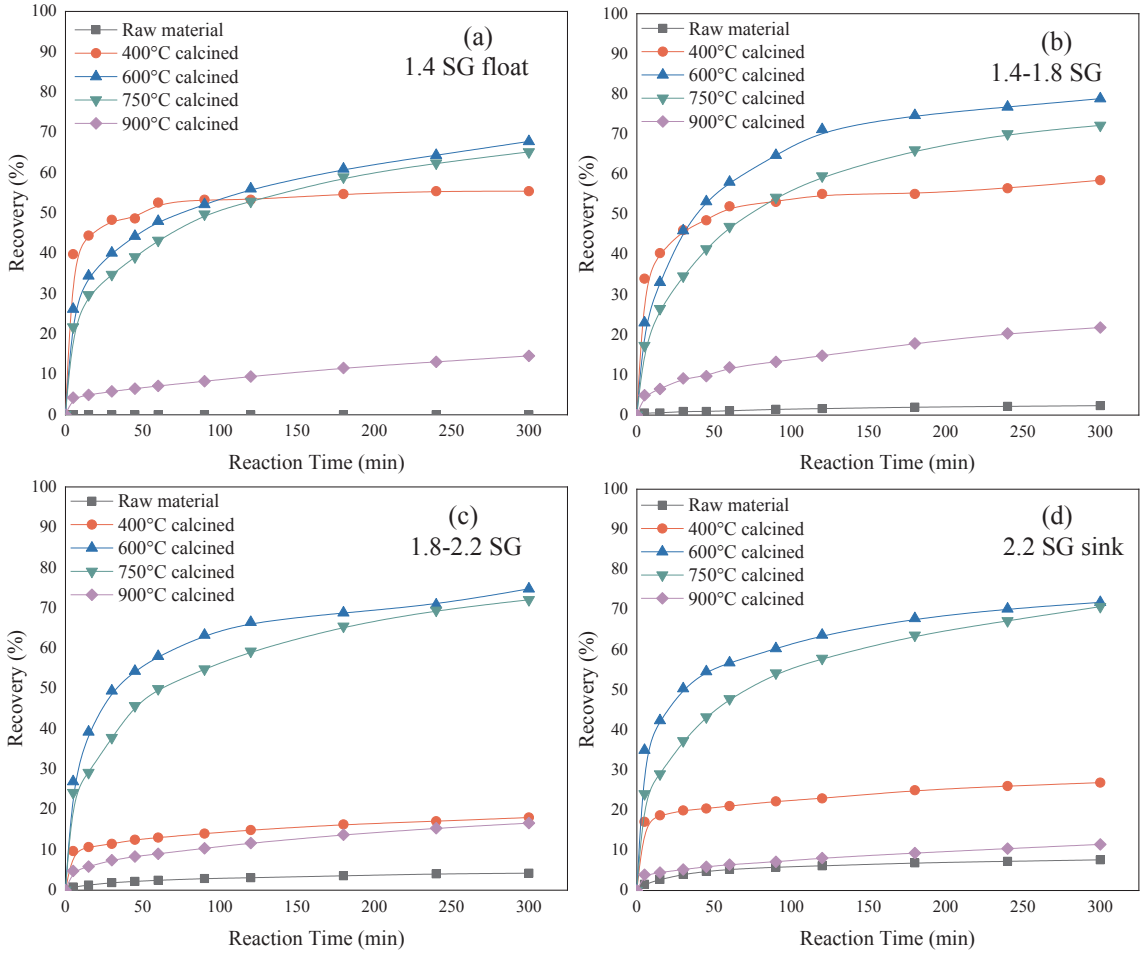

Fig. 4. Leaching recoveries of lithium from the different SG fractions of the Baker coal as a function of reaction time.

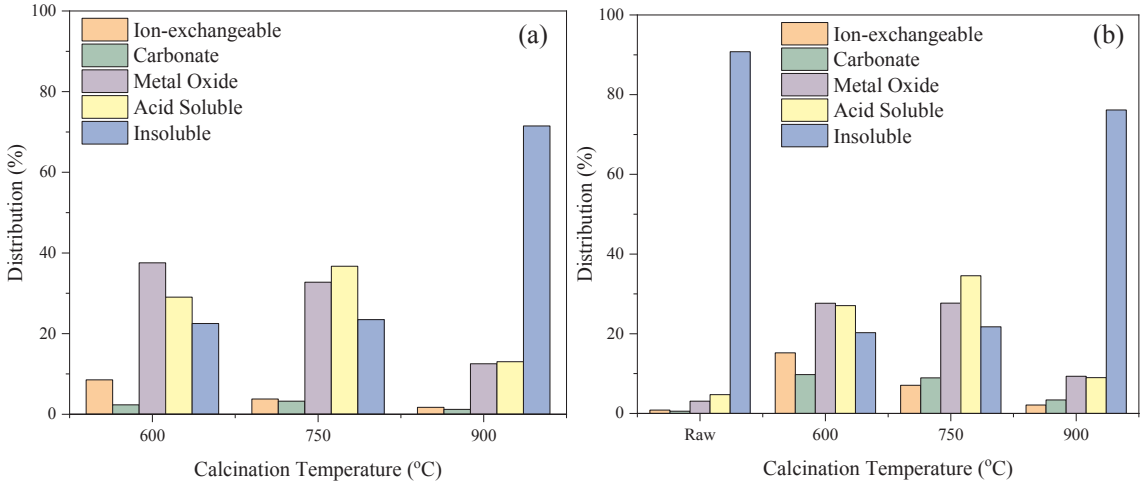

Fig. 5. Distributions of lithium in different modes of occurrence in the raw and calcined materials: (a) 1.4 SG float fraction; (b) 2.2 SG sink fraction.

The diffraction peaks of kaolinite disappeared for both the 1.4 SG float and 2.2 SG sink materials after calcination under 600 °C. This phenomenon has been observed in prior studies [17,29,30], which can be explained by the dehydration and decomposition of the layered kaolinite structures [37,38]. The diffraction peaks of illite and muscovite were still detectable in the 600 °C calcination products, indicating that these mineral crystals were not destroyed during calcination. However, as reported by Guggenheim et al. [39] and Irassar et al. [40], dehydroxylation and crystal expansion of illite and muscovite is initiated at relatively low temperatures (e.g., 300 °C) despite the fact that their mineral phases remain unchanged until 850–900 °C. The enhanced leaching recovery of lithium after calcination under 600–750 °C may be caused by the dehydration and disintegration of kaolinite as well as dehydroxylation and expansion of muscovite and illite.

Based on the prevalence of clays (kaolinite, illite, and mica) in the materials, it can be concluded that aluminum and potassium occurring in the materials are primarily associated with the clays. Therefore,

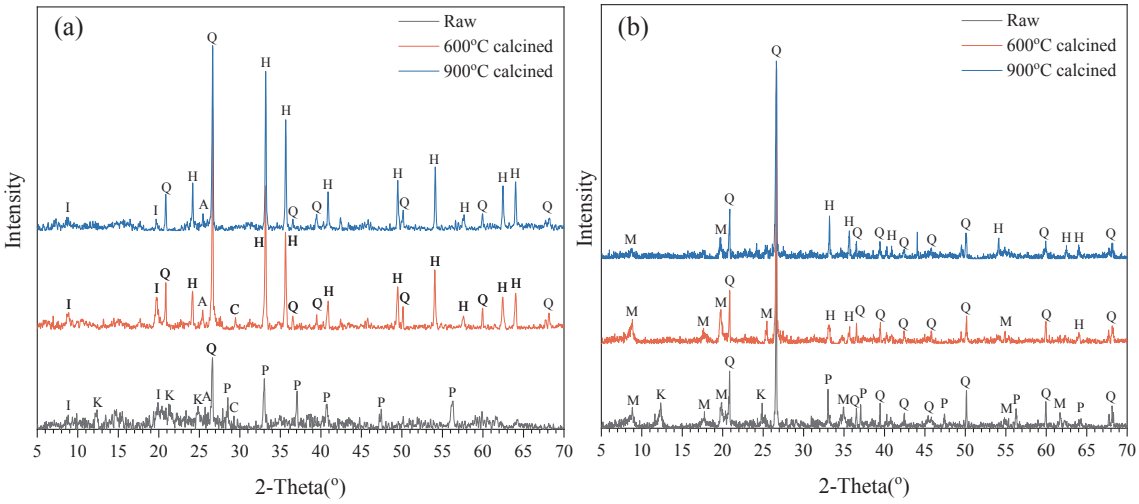

Fig. 6. XRD patterns of the raw, 600 °C calcined, and 900 °C calcined samples of the (a) 1.4 SG float and (b) 2.2 SG sink fractions. (A-anatase, C-calcite, H-hematite, I-illite, K-kaolinite, M-muscovite, Q-quartz).

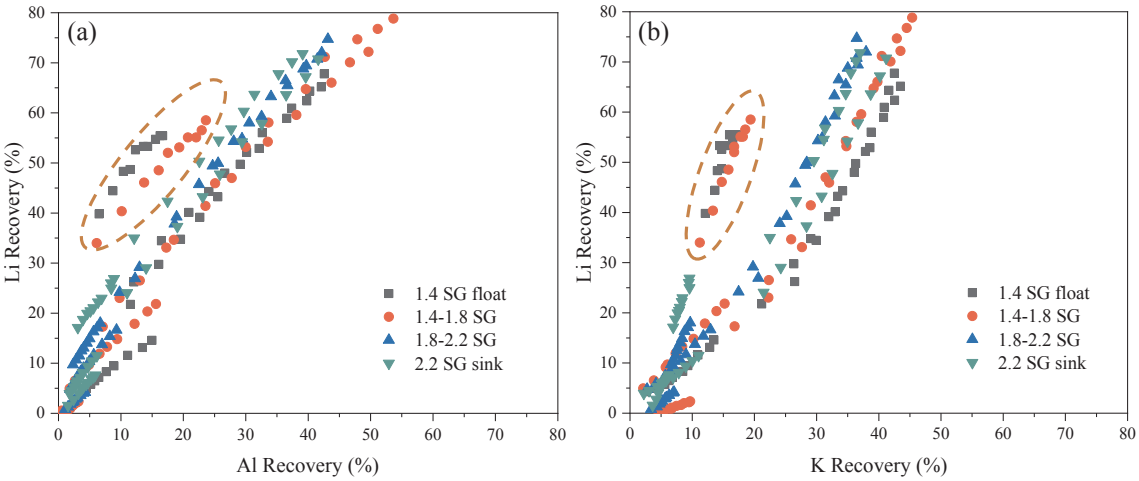

Fig. 7. Correlation between lithium recovery and the recovery of (a) aluminum and (b) potassium for the density fractionized samples; circled results show Li, Al and K recoveries from the 400 °C calcination products of the 1.4 SG float and 1.4–1.8 SG fractions.

Table 2
Linear fitting parameters for Li versus Al leaching kinetic data.

Calcination Temperature	Fitting Parameters	Density fractions			
		1.4 SG Float	1.4–1.8 SG	1.8–2.2 SG	2.2 SG Sink
Untreated	Equation	NA	$y = 0.67x$	$y = 0.99x$	$y = 1.29x$
	R^2_{adj}	NA	0.975	0.998	0.999
400 °C	Equation	$y = 3.87x$	$y = 2.75x$	$y = 3.01x$	$y = 3.41x$
	R^2_{adj}	0.974	0.971	0.986	0.970
600 °C	Equation	$y = 1.70x$	$y = 1.60x$	$y = 1.82x$	$y = 2x$
	R^2_{adj}	0.993	0.993	0.996	0.991
750 °C	Equation	$y = 1.64x$	$y = 1.56x$	$y = 1.83x$	$y = 1.78x$
	R^2_{adj}	0.997	0.992	0.994	0.997
900 °C	Equation	$y = 1.03x$	$y = 1.52x$	$y = 1.98x$	$y = 1.99x$
	R^2_{adj}	0.997	0.981	0.989	0.997

information regarding the modes of occurrence of lithium may be obtained by analyzing the aluminum and potassium leaching characteristics. As shown in Fig. 7(a) and (b), a strong linear correlation exists between lithium and aluminum as well as potassium leaching recoveries. This can be confirmed by the fact that adjusted coefficient of determination (R^2_{adj}) values of the linear fittings shown in Table 2 and Table 3 are greater than 0.94. The strong linear correlation further supports the conclusion that lithium in the Baker materials is mainly associated with clays, and changes to the clay crystal structures caused by calcination increase lithium leachability. Fig. 7(a) and (b) also shows that, at the same level of aluminum or potassium recovery, higher lithium recoveries were obtained from the 400 °C calcination products of

Table 3
Linear fitting parameters for Li versus K leaching kinetic data.

Calcination Temperature	Fitting Parameters	Density Fractions			
		1.4 SG Float	1.4–1.8 SG	1.8–2.2 SG	2.2 SG Sink
Untreated	Equation	NA	$y = 0.19x$	$y = 0.51x$	$y = 1.05x$
	R^2_{adj}	NA	0.946	0.960	0.960
400 °C	Equation	$y = 3.4x$	$y = 3.07x$	$y = 1.73x$	$y = 2.66x$
	R^2_{adj}	0.9981	0.999	0.994	0.999
600 °C	Equation	$y = 1.39x$	$y = 1.62x$	$y = 1.87x$	$y = 1.81x$
	R^2_{adj}	0.985	0.986	0.991	0.996
750 °C	Equation	$y = 1.36x$	$y = 1.55x$	$y = 1.79x$	$y = 1.54x$
	R^2_{adj}	0.990	0.989	0.994	0.987
900 °C	Equation	$y = 1.05x$	$y = 1.49x$	$y = 1.30x$	$y = 1.07x$
	R^2_{adj}	0.996	0.996	0.998	0.991

the 1.4 SG float and 1.4–1.8 SG fractions relative to the other materials. This result may suggest that some of the lithium present in the low ash coals was associated with the organic matter. After the organic matter was removed by calcination, the organically-associated lithium was released and easily leached, which agrees with the acid leaching test results (see Fig. 4(a) and (b)). Despite that some mineral components were also exposed after calcination under 400 °C, the dehydration of kaolinite and the dehydroxylation of illite were insufficient, and thus aluminum recoveries were relatively low.

The acid leaching test and sequential chemical extraction results (see Fig. 4(a)-(d) and Fig. 5(a) and (b)) collectively showed that the leaching performance of lithium from the density fractionized samples deteriorated when the calcination temperature exceeded 600 °C. The reduction in performance can be explained by the fact that, after complete dehydration and disintegration at 600–700 °C, amorphous meta-kaolinite starts to recrystallize by re-linking the octahedrally coordinated Al with the tetrahedrally coordinated Si [41]. Recrystallization results in sintering of the meta-kaolinite, thus decreasing the surface area and porosity [17]. Therefore, lithium present in the coal materials was encapsulated in the sintered meta-kaolinite structures after calcination under high temperatures such as 900 °C. The morphologies of the 600 °C and 900 °C calcination products of the 1.4 SG float material are shown in Fig. 8(a) and(b). Aluminum silicate slices with thicknesses of several nanometers were found in the 600 °C calcined material. However, in the 900 °C calcined material, the aluminum silicate slices were linked together due to sintering.

3.4. Leaching kinetic analysis

To better understand the reaction rates and leaching mechanisms, the data plotted in Fig. 4(a)–(d) were analyzed by fitting the data to standard kinetic models. Since the recovery of lithium from the raw materials was negligible, the kinetic analyses were only performed on the calcined materials. Initially, the shrinking core model, a common equation used to describe multiphase solid–liquid processes, was used to fit the data [42,43]. According to the model, if the reaction rate is controlled by diffusion through the solid layer, the integral rate expression is as follows:

$$1 - \frac{2}{3}\alpha - (1 - \alpha)^{2/3} = K_d t \tag{3}$$

where K_d represents the pore diffusion rate constant, α leach recovery in decimal, and t reaction time. Alternatively, if the reaction rate is controlled by the surface chemical reaction, the integral rate equation can be expressed as follows:

$$1 - (1 - \alpha)^{1/3} = K_c t \tag{4}$$

where K_c represents the surface chemical rate constant.

The rate constants and the corresponding adjusted coefficient of determination (R^2_{adj}) values for the shrinking core diffusion and chemical reaction models are shown in Table 4 and Table 5, respectively. As indicated by the R^2_{adj} values, the extraction of lithium from the calcined materials can be more accurately fitted by the diffusion model relative to the chemical reaction model. Therefore, the data suggests

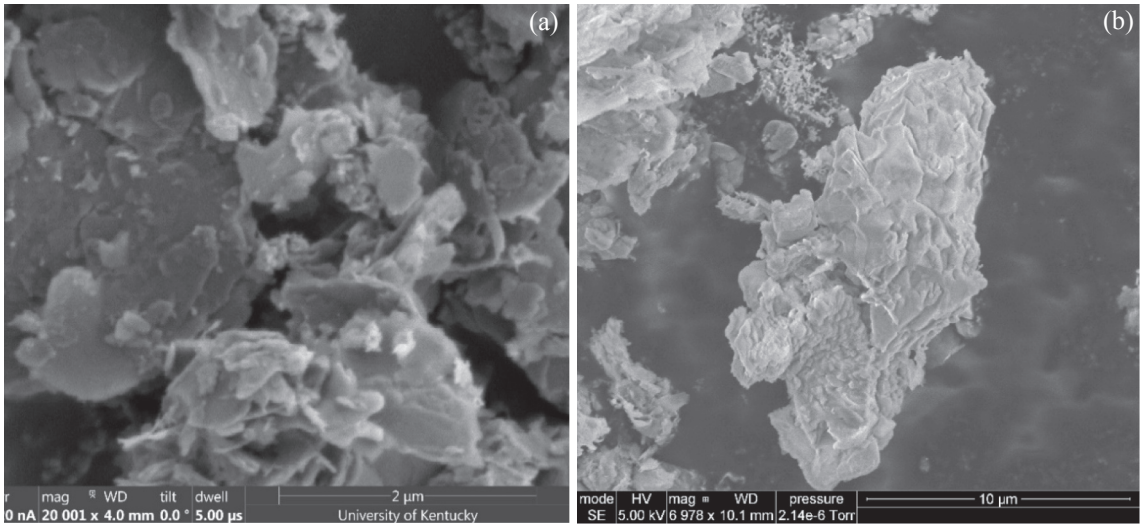

Fig. 8. SEM images of (a) 600 °C and (b) 900 °C calcination products of the 1.4 SG float material.

Table 4
K_d and R^2_{adj} for the shrinking core diffusion model (see Eq. 1).

Sample	400 °C Calcined		600 °C Calcined		750 °C Calcined		900 °C Calcined	
	$K_d(\times 10^{-4})$	R^2_{adj}	$K_d(\times 10^{-4})$	R^2_{adj}	$K_d(\times 10^{-4})$	R^2_{adj}	$K_d(\times 10^{-4})$	R^2_{adj}
1.4 SG Float	2.30	0.6853	3.06	0.9313	2.75	0.9535	0.086	0.9942
1.4–1.8 SG	2.43	0.7574	4.96	0.9231	3.62	0.9679	0.21	0.9930
1.8–2.2 SG	0.16	0.8599	4.19	0.8833	3.61	0.9539	0.12	0.9845
2.2 SG Sink	0.40	0.7906	3.91	0.8665	3.38	0.9558	0.055	0.9760

that the leaching kinetics of lithium from the calcined materials were not controlled by the surface chemical reactions but rather by diffusion.

Fig. 9 (a)-(d) show the linear fitting results using the shrinking core diffusion model. This data indicates that the experimental results of the 750 °C and 900 °C calcined materials can be well fitted using the inner diffusion model with an R^2_{adj} more than 0.95. For the 600 °C calcined materials and particularly the higher density fractions, the fitting outcomes were not as accurate as indicated by the relatively low R^2_{adj} values (e.g., 0.87 for 2.2 SG sink). Finally, both the diffusion and the chemical reaction models failed to fit the 400 °C calcined materials.

A new variant of shrinking core model developed by Dickinson and Heal [44] was used to fit the leaching results to find a better model. The model was derived based on the dissolution reaction of a sphere solid particle in liquid (Fig. 10). Assuming the original radius of the particle equals r_0, after reacting for time t, the radius is decreased to r (namely$r = r_0 - x$) and the solid–liquid interface moves inwards a distance x. Based on the description, the fraction of unreacted solid on a volume basis is

$$(1-\alpha) = \frac{(4/3)\pi(r_0-x)^3}{(4/3)\pi(r_o)^3} = \frac{(r_0-x)^3}{(r_o)^3} \tag{5}$$

$$(1-\alpha)^{1/3} = \frac{r_0-x}{r_0} = 1 - \frac{x}{r_0} \tag{6}$$

$$\frac{x}{r_0} = 1-(1-\alpha)^{1/3} \tag{7}$$

$$x = r_0(1-(1-\alpha)^{1/3}) \tag{8}$$

$$\frac{dx}{d\alpha} = \frac{1}{3}r_0(1-\alpha)^{-2/3} \tag{9}$$

Furthermore, diffusion across the product layer shown in Fig. 10 is assumed to follow the parabolic diffusion law, which defines that the rate of reaction is inversely proportional to the product layer thickness:

$$\frac{dx}{dt} = \frac{DV_mC_0}{x} \tag{10}$$

where x is the thickness of the product layer, D the diffusion coefficient (slowest transport), V_m the volume of product layer formed from 1 mol of the slowest penetrating component, and C_0 the concentration of the penetrating species at the surface. When the diffusion across the product layer and the transfer across the contacting surface both control the rate,

$$\frac{dx}{dt} = \frac{DV_mC_0}{x}\bullet 4\pi r^2 = k_v\frac{r^2}{x} \tag{11}$$

where $k_v = 4\pi DV_mC_0$,

$$\frac{x\,dx}{r^2} = k_v\,dt \tag{12}$$

Substituting for x, dx, and r^2 gives

$$\frac{1}{3}((1-\alpha)^{-4/3} - (1-\alpha)^{-1})d\alpha = k_v dt \tag{13}$$

Integrating the above equation gives

$$\frac{1}{3}(3(1-\alpha)^{-1/3} + \ln(1-\alpha) + c) = k_v t \tag{14}$$

When t equals 0, $\alpha = 0$ and $c = -3$. Therefore, the following expression can be obtained:

$$\frac{1}{3}ln(1-\alpha) - 1 + (1-\alpha)^{-1/3} = K_v t \tag{15}$$

where K_v is the apparent rate constant. As shown in Table 6, the new variant model fits the data better than the inner diffusion model especially for the 750 °C and 900 °C calcined materials. Therefore, the leaching rate of lithium from the materials that was calcined under 600–900 °C was controlled by the interfacial transfer and diffusion across the product layer. For all density fractions, the apparent rate constant, K_v, was decreased when the temperature exceeded 600 °C, which agrees with the finding that final recoveries of lithium from the 750 °C and 900 °C calcined materials were lower than those of the 600 °C calcined materials (see Fig. 4). The fitting results indicated that calcination impacted the association characteristics of lithium the density fractionated samples. The model proposed by Dickinson and Heal [44] describes the scenario when the interface transfer (i.e., contacting area) and diffusion through product layer (i.e., product layer thickness) control leaching rate, which indicates that the contacting surface area change during leaching is significant due to the blockage and product layer formation. At 600 °C calcination, the dehydration and disintegration of clay structure benefited the interface mass transfer due to large surface area. However, sintering of the clays occurred when the samples were calcined under 900 °C, which reduced contacting area and created blockage, and the dissolution of the sintered clays formed thicker product layer that limited the diffusion process.

Based on the trend of the data points shown in Fig. 11, the leaching process of the 600 °C calcination products especially the 1.8–2.2 SG and 2.2 SG sink fractions can be divided into two stages, i.e., quick reactions

Table 5
K_c and R^2_{adj} for the shrinking chemical reaction model (see Eq. (2)).

Sample	400 °C Calcined		600 °C Calcined		750 °C Calcined		900 °C Calcined	
	$K_c(\times 10^{-3})$	R^2_{adj}	$K_c(\times 10^{-3})$	R^2_{adj}	$K_c(\times 10^{-3})$	R^2_{adj}	$K_c(\times 10^{-3})$	R^2_{adj}
1.4 SG Float	1.18	0.6196	1.38	0.8039	1.29	0.8328	0.21	0.8756
1.4–1.8 SG	1.22	0.6687	1.82	0.8273	1.15	0.8701	0.33	0.8816
1.8–2.2 SG	0.29	0.7170	1.65	0.7758	1.50	0.8413	0.25	0.8533
2.2 SG Sink	0.47	0.6701	1.59	0.7507	1.45	0.8408	0.17	0.8320

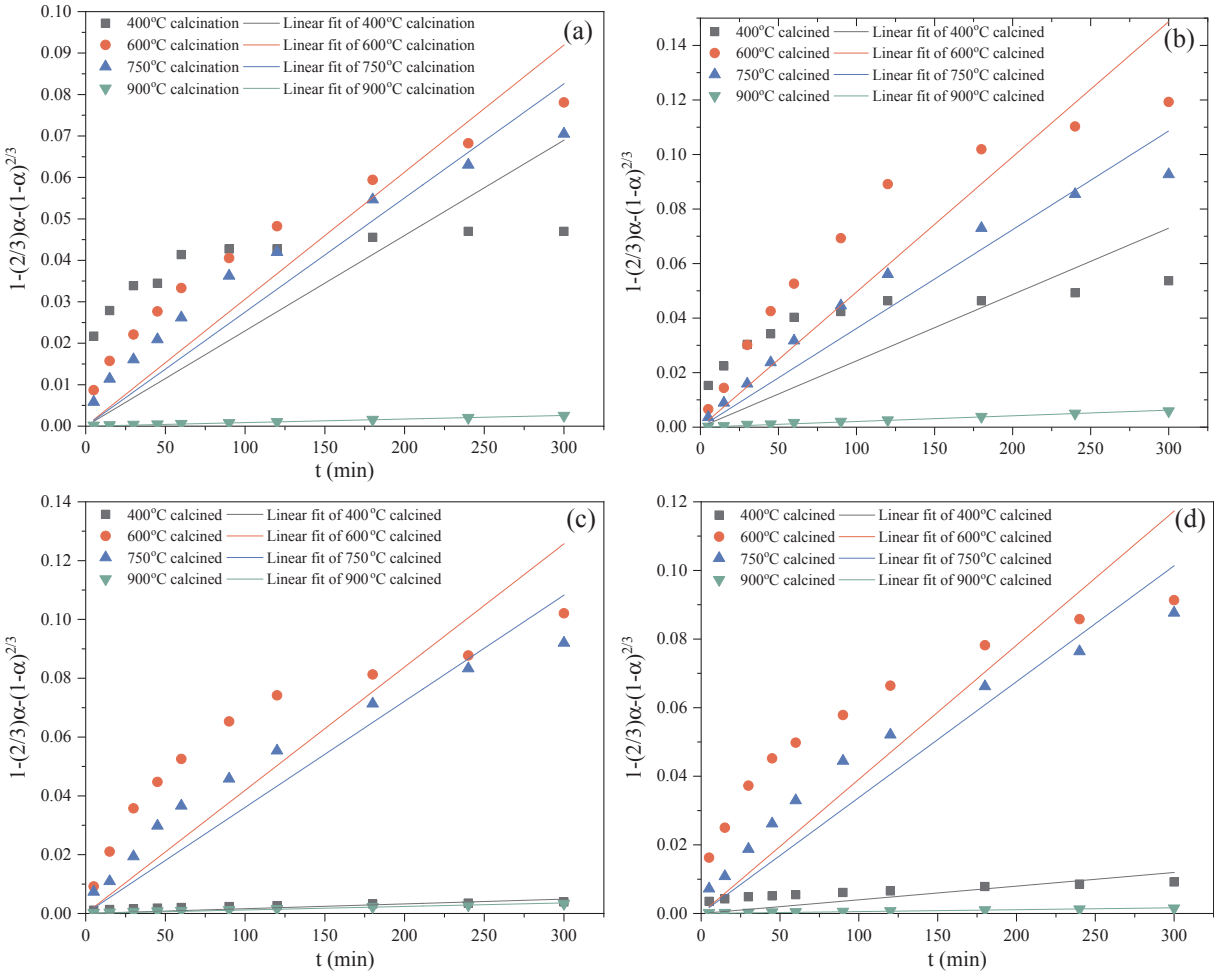

Fig. 9. Variance of $1 - \frac{2}{3}\alpha - (1-\alpha)^{2/3}$ between the experimental data and model predictions as a function of leaching time for the samples that were calcined under different temperatures: (a) 1.4 SG float, (b) 1.4–1.8 SG, (c) 1.8–2.2 SG, and (d) 2.2 SG sink.

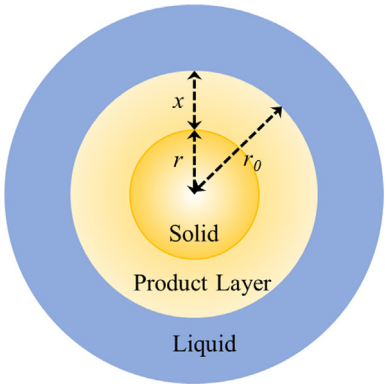

Fig. 10. Schematic representation of the leaching of a sphere solid particle in liquid.

at the beginning and slow reactions at the end. The slow reactions might be due to (1) insufficient dehydroxylation and crystal expansion of muscovite and/or (2) recrystallization of meta-kaolinite. For the 400 °C calcined materials, none of the above models satisfactorily fitted the experimental results, which indicates a complex reaction process.

4. Conclusions

This study investigated the leaching recovery of lithium from different SG fractions (1.4 SG sink, 1.4–1.8 SG, 1.8–2.2 SG, and 2.2 SG sink) of the Baker seam coal. Proximate and elemental analyses showed that the 1.8–2.2 SG and 2.2 SG sink fractions contained 185 ppm and 150 ppm of lithium, respectively, when reported on a whole sample basis. Due to the high lithium contents and mass distribution, nearly 90% of the lithium present in the coal existed in these two density fractions. This distribution creates an opportunity to recover lithium from the Baker material without sacrificing the value of clean coal.

Acid leaching tests showed that lithium recoveries from the raw materials of the four density fractions was minimal (less than 10%) when using standard experimental conditions of 1.2 M HCl and 75 °C reaction temperature. However, after calcination under proper temperatures (e.g., 600 °C), the recoveries were increased to 70–80%. Sequential chemical extraction tests showed that, in the 2.2 SG sink raw material, 91% of the lithium occurred as insoluble forms which were not dissolved even under strong acidic and oxidizing environments (e.g., 15 mL concentrated nitric acid plus 40 mL hydrogen peroxide). After calcination under 600 °C for two hours, the majority of the insoluble lithium was converted to more soluble forms such as carbonates and metal oxides. The sequential chemical extraction findings agreed well with the acid leaching test results.

Mineralogy characterization by XRD analysis showed that quartz, kaolinite, illite, muscovite, and pyrite were the dominant mineral phases present in the Baker materials. X-ray diffraction peaks of kaolinite disappeared after calcination under 600 °C due to the dehydration and disintegrations of layered kaolinite structures. Despite that muscovite and illite were still detectable after calcination, dehydroxylation

Table 6
K_v and R^2_{adj} for the model developed by Dickinson and Heal [44] (see Equation (15)).

Sample	400 °C Calcined		600 °C Calcined		750 °C Calcined		900 °C Calcined	
	$K_v(\times 10^{-4})$	R^2_{adj}	$K_v(\times 10^{-4})$	R^2_{adj}	$K_v(\times 10^{-4})$	R^2_{adj}	$K_v(\times 10^{-4})$	R^2_{adj}
1.4 SG Float	1.92	0.7240	2.92	0.9787	2.53	0.9880	0.047	0.9958
1.4–1.8 SG	2.07	0.8046	6.07	0.9758	3.78	0.9951	0.12	0.9963
1.8–2.2 SG	0.092	0.8737	4.58	0.9488	3.73	0.9924	0.067	0.9890
2.2 SG Sink	0.24	0.8128	4.10	0.9363	3.39	0.9926	0.030	0.9800

and expansion of their crystals were expected to occur per literature. A strong linear correlation was observed between the lithium and aluminum recoveries indicating the association of lithium with the clay minerals. Therefore, the positive effects of calcination on lithium leaching recovery was explained by the dehydration and disintegration of kaolinite as well as the dehydroxylation and expansion of muscovite/illite.

Kinetic analysis of the acid leaching results showed that the leaching rate of lithium in all the SG fractions calcined under 600–900 °C was controlled by the interface transfer and diffusion across the product layer. The rate significantly decreased when the calcination temperature exceeded 600 °C. This can be explained by the recrystallization and sintering of clays at high temperatures, which reduced contacting surface area and created blockage, and the dissolution of the sintered clays formed thicker product layer that limited the diffusion process. All the factors contributed to the lower recovery of lithium from the materials calcined at > 600 °C. Altogether, these results suggest that, after proper roasting, lithium can be co-extracted with rare earths and other critical materials into a pregnant leach solution. If properly recovered, this additional byproduct may bolster the economic viability of trace metal recovery from coal refuse and ultimately support more sustainable uses of this large waste stream.

Credit authorship contribution statement

Wencai Zhang: Conceptualization, Methodology, Validation, Investigation, Writing - original draft. **Aaron Noble:** Formal analysis, Writing - review & editing. **Xinbo Yang:** Methodology, Writing - review & editing. **Rick Honaker:** Resources, Writing - review & editing, Supervision, Project administration, Funding acquisition.

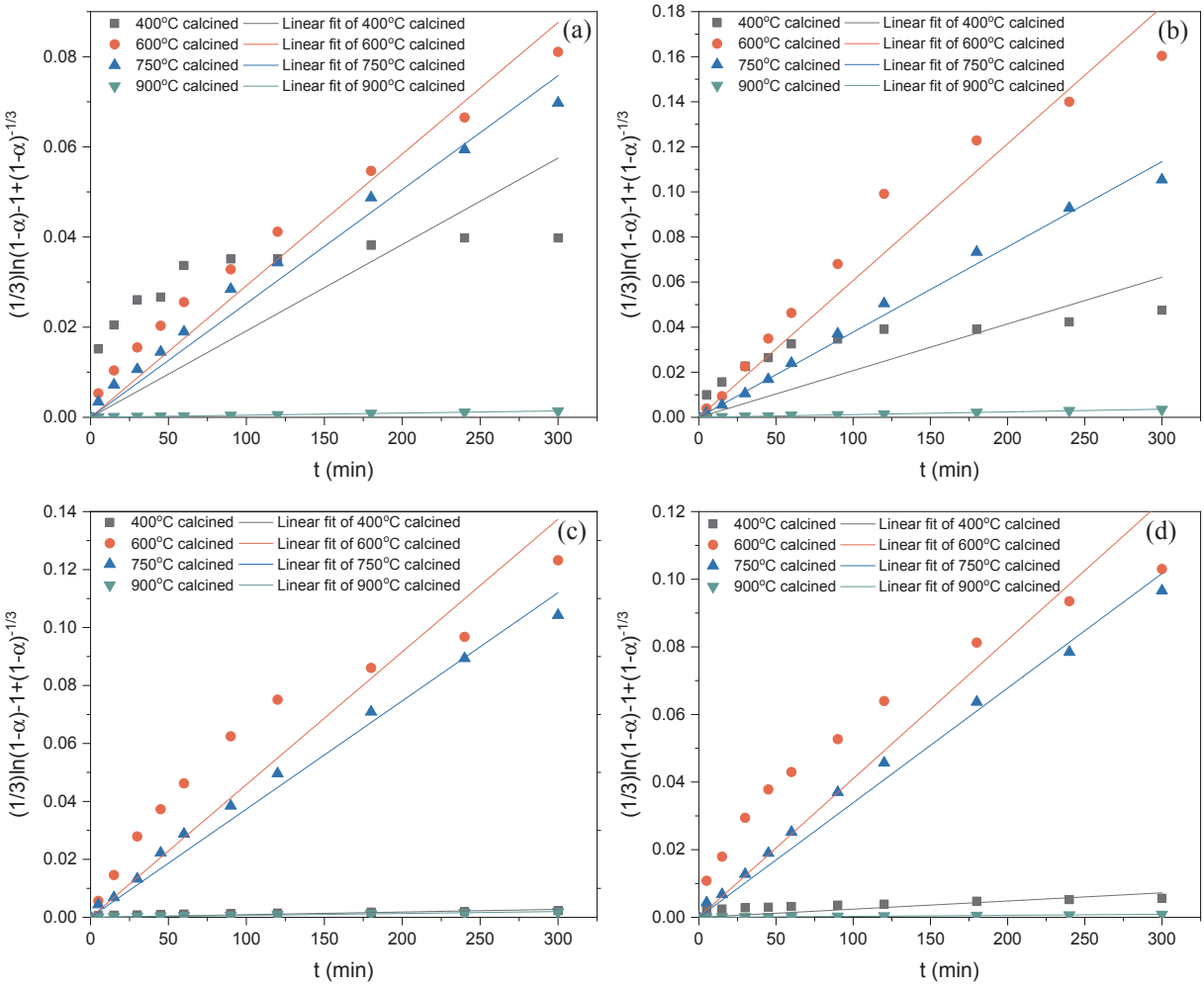

Fig. 11. Variation of $\frac{1}{3}ln(1-\alpha)-1+(1-\alpha)^{-1/3}$ in the Dickenson and Heal model as a function of leaching duration for the samples that were calcined under different temperatures.

Acknowledgement

This material is based upon work supported by the Department of Energy under Award Number DE-FE0027035. Disclaimer: This report was prepared as an account of work sponsored by an agency of the United States Government. Neither the United States Government nor any agency thereof, nor any of their employees, makes any warranty, express or implied, or assumes any legal liability or responsibility for the accuracy, completeness, or usefulness of any information, apparatus, product, or process disclosed, or represents that its use would not infringe privately owned rights. Reference herein to any specific commercial product, process, or service by trade name, trademark, manufacturer, or otherwise does not necessarily constitute or imply its endorsement, recommendation, or favoring by the United States Government or any agency thereof. The views and opinions of authors expressed herein do not necessarily state or reflect those of the United States Government or any agency thereof.

Declaration of interests

None.

References

[1] Survey USG. Mineral Commodity Summaries, 2009. Government Printing Office; 2019.
[2] Zhang Y, Hu Y, Wang L, Sun W. Systematic review of lithium extraction from salt-lake brines via precipitation approaches. Miner Eng 2019;139:105868https://doi.org/10.1016/j.mineng.2019.105868.
[3] Zhao X, Yang H, Wang Y, Sha Z. Review on the electrochemical extraction of lithium from seawater/brine. J Electroanal Chem 2019;850:113389https://doi.org/10.1016/j.jelechem.2019.113389.
[4] D. Trump, A Federal Strategy to Ensure Secure and Reliable Supplies of Critical Minerals, Donald Trump, Washington, DC, Accessed Apr. 3 (2018) 2018.
[5] Liu G, Zhao Z, Ghahreman A. Novel approaches for lithium extraction from salt-lake brines: A review. Hydrometallurgy 2019;187:81–100. https://doi.org/10.1016/j.hydromet.2019.05.005.
[6] Bernhardt D, Reilly II JF. Mineral commodity summaries 2019. Reston, USA: US Geol. Surv; 2019.
[7] McLellan B, Corder G, Ali S, Golev A. Rare metals, unconventional resources, and sustainability. Geol Soc Am Spec Pap 2016;520:57–65.
[8] Ambrose H, Kendall A. Understanding the future of lithium: Part 2, temporally and spatially resolved life-cycle assessment modeling. J Ind Ecol 2019:1–11. https://doi.org/10.1111/jiec.12942.
[9] Seredin VV, Dai S, Sun Y, Chekryzhov IY. Coal deposits as promising sources of rare metals for alternative power and energy-efficient technologies. Appl Geochem 2013;31:1–11. https://doi.org/10.1016/j.apgeochem.2013.01.009.
[10] Seredin VV, Dai S. Coal deposits as potential alternative sources for lanthanides and yttrium. Int J Coal Geol 2012;94:67–93. https://doi.org/10.1016/j.coal.2011.11.001.
[11] Dai S, Finkelman RB. Coal as a promising source of critical elements: Progress and future prospects. Int J Coal Geol 2018;186:155–64. https://doi.org/10.1016/j.coal.2017.06.005.
[12] Honaker RQ, Groppo J, Yoon R-H, Luttrell GH, Noble A, Herbst J. Process evaluation and flowsheet development for the recovery of rare earth elements from coal and associated byproducts. Miner Metall Process 2017;34:107–15. https://doi.org/10.19150/mmp.7610.
[13] Vass CR, Noble A, Ziemkiewicz PF. The occurrence and concentration of rare earth elements in acid mine drainage and treatment by-products: Part 1—Initial survey of the northern Appalachian Coal Basin. Mining Metall Explor 2019:917–29. https://doi.org/10.1007/s42461-019-0097-z.
[14] Lin R, Howard BH, Roth EA, Bank TL, Granite EJ, Soong Y. Enrichment of rare earth elements from coal and coal by-products by physical separations. Fuel 2017;200:506–20. https://doi.org/10.1016/j.fuel.2017.03.096.
[15] Laudal DA, Benson SA, Addleman RS, Palo D. Leaching behavior of rare earth elements in Fort Union lignite coals of North America. Int J Coal Geol 2018;191:112–24. https://doi.org/10.1016/j.coal.2018.03.010.
[16] Honaker RQ, Zhang W, Werner J, Noble A, Luttrell GH, Yoon R-H. Enhancement of a process flowsheet for recovering and concentrating critical materials from bituminous coal sources. Mining Metall Explor 2019. accepted.
[17] Zhang W, Honaker R. Calcination pretreatment effects on acid leaching characteristics of rare earth elements from middlings and coarse refuse material associated with a bituminous coal source. Fuel 2019;249:130–45. https://doi.org/10.1016/j.fuel.2019.03.063.
[18] Yang X, Werner J, Honaker RQ. Leaching of rare Earth elements from an Illinois basin coal source. J Rare Earths 2019;37:312–21. https://doi.org/10.1016/j.jre.2018.07.003.
[19] Huang Q, Noble A, Herbst J, Honaker R. Liberation and release of rare earth minerals from Middle Kittanning, Fire Clay, and West Kentucky No. 13 coal sources. Powder Technol 2018;332:242–52. https://doi.org/10.1016/j.powtec.2018.03.063.
[20] King JF, Taggart RK, Smith RC, Hower JC, Hsu-Kim H. Aqueous acid and alkaline extraction of rare earth elements from coal combustion ash. Int J Coal Geol 2018;195:75–83. https://doi.org/10.1016/j.coal.2018.05.009.
[21] Wang Z, Dai S, Zou J, French D, Graham IT. Rare earth elements and yttrium in coal ash from the Luzhou power plant in Sichuan, Southwest China: Concentration, characterization and optimized extraction. Int J Coal Geol 2019;203:1–14. https://doi.org/10.1016/j.coal.2019.01.001.
[22] Stuckman MY, Lopano CL, Granite EJ. Distribution and speciation of rare earth elements in coal combustion by-products via synchrotron microscopy and spectroscopy. Int J Coal Geol 2018;195:125–38. https://doi.org/10.1016/j.coal.2018.06.001.
[23] Vass CR, Noble A, Ziemkiewicz PF. The occurrence and concentration of rare earth elements in acid mine drainage and treatment byproducts. Part 2: Regional survey of northern and central Appalachian Coal Basins. Mining Metall Explor 2019:1.
[24] FOA, Process Scale-up and Optimization/Efficiency Improvements for Rare Eearth Elements (REE) and Critical Materials (CM) Recovery From United States Coal-Based Resources, Funding Oppor. Announc. Number DE-FOA-0002003, 2019.
[25] Ketris MP, Yudovich YE. Estimations of Clarkes for Carbonaceous biolithes: World averages for trace element contents in black shales and coals. Int J Coal Geol 2009;78:135–48. https://doi.org/10.1016/j.coal.2009.01.002.
[26] Sun Y, Li Y, Zhao C, Lin M, Wang J, Qin S. Concentrations of lithium in Chinese coals. Energy Explor Exploit 2010;28:97–104. https://doi.org/10.1260/0144-5987.28.2.97.
[27] Dai S, Jiang Y, Ward CR, Gu L, Seredin VV, Liu H, et al. Mineralogical and geochemical compositions of the coal in the Guanbanwusu Mine, Inner Mongolia, China: Further evidence for the existence of an Al (Ga and REE) ore deposit in the Jungar Coalfield. Int J Coal Geol 2012;98:10–40. https://doi.org/10.1016/j.coal.2012.03.003.
[28] Finkelman RB, Palmer CA, Wang P. Quantification of the modes of occurrence of 42 elements in coal. Int J Coal Geol 2018;185:138–60. https://doi.org/10.1016/j.coal.2017.09.005.
[29] Zhang W, Honaker R. Enhanced leachability of rare earth elements from calcined products of bituminous coals. Miner Eng 2019;142:105935https://doi.org/10.1016/j.mineng.2019.105935.
[30] Honaker RQ, Zhang W, Werner J. Acid leaching of rare earth elements from coal and coal ash: implications for using fluidized bed combustion to assist in the recovery of critical materials. Energy Fuels 2019;33:5971–80. https://doi.org/10.1021/acs.energyfuels.9b00295.
[31] Huggins FE. Overview of analytical methods for inorganic constituents in coal. Int J Coal Geol 2002;50:169–214. https://doi.org/10.1016/S0166-5162(02)00118-0.
[32] Chou JD, Wey MY, Chang SH. Evaluation of the distribution patterns of Pb, Cu and Cd from MSWI fly ash during thermal treatment by sequential extraction procedure. J Hazard Mater 2009;162:1000–6. https://doi.org/10.1016/j.jhazmat.2008.05.155.
[33] Pan J, Zhou C, Tang M, Cao S, Liu C, Zhang N, et al. Study on the modes of occurrence of rare earth elements in coal fly ash by statistics and a sequential chemical extraction procedure. Fuel 2019;237:555–65. https://doi.org/10.1016/j.fuel.2018.09.139.
[34] Lin R, Stuckman M, Howard BH, Bank TL, Roth EA, Macala MK, et al. Application of sequential extraction and hydrothermal treatment for characterization and enrichment of rare earth elements from coal fly ash. Fuel 2018;232:124–33. https://doi.org/10.1016/j.fuel.2018.05.141.
[35] ASTM D5142-2009: Standard Test Methods for Proximate Analysis of the Analysis Sample of Coal and Coke by Instrumental Procedures, n.d.
[36] Zhang W, Honaker RQ. Rare earth elements recovery using staged precipitation from a leachate generated from coarse coal refuse. Int J Coal Geol 2018;195:189–99. https://doi.org/10.1016/j.coal.2018.06.008.
[37] Cao Z, Cao Y, Dong H, Zhang J, Sun C. Effect of calcination condition on the microstructure and pozzolanic activity of calcined coal gangue. Int J Miner Process 2016;146:23–8. https://doi.org/10.1016/j.minpro.2015.11.008.
[38] Yagüe S, Sánchez I, De La Villa RV, García-Giménez R, Zapardiel A, Frías M. Coal-mining tailings as a pozzolanic material in cements industry. Minerals 2018;8:1–13. https://doi.org/10.3390/min8020046.
[39] Guggenheim S, Chang YH, Koster Van Groos AF. Muscovite dehydroxylation: high-temperature studies. Am Mineral 1987;72:537–50.
[40] Irassar EF, Bonavetti VL, Castellano CC, Trezza MA, Rahhal VF, Cordoba G, et al. Calcined illite-chlorite shale as supplementary cementing material: Thermal treatment, grinding, color and pozzolanic activity. Appl Clay Sci 2019;179:105143https://doi.org/10.1016/j.clay.2019.105143.
[41] Wan Q, Rao F, Song S. Reexamining calcination of kaolinite for the synthesis of metakaolin geopolymers – roles of dehydroxylation and recrystallization. J Non Cryst Solids 2017;460:74–80. https://doi.org/10.1016/j.jnoncrysol.2017.01.024.
[42] Levenspiel O. Chemical reaction engineering. New York: John Wiley & Sons Inc; 1972.
[43] Mashifana T, Ntuli F, Okonta F. Leaching kinetics on the removal of phosphorus from waste phosphogypsum by application of shrinking core model. South Afr J Chem Eng 2019;27:1–6. https://doi.org/10.1016/j.sajce.2018.11.001.
[44] Dickinson CF, Heal GR. Solid-liquid diffusion controlled rate equations. Thermochim Acta 1999;340–341:89–103. https://doi.org/10.1016/s0040-6031(99)00256-7.